PAPER

Check for updates

Differential pulse voltametric detection of dopamine using polyaniline-functionalized graphene oxide/silica nanocomposite for point-of-care diagnostics†

Ankita Tejwani, [ID] Urvashi Sonkar, [ID] Kamlesh Shrivas, [ID] * Khushali Tandey, [ID] Indrapal Karbhal, [ID] Manas Kanti Deb [ID] and Shamsh Pervez [ID]

In this study, a novel composite material, GO/SiO$_2$@PANI, was synthesized and employed as an electrochemical sensor for the detection of dopamine in urine using differential pulse voltammetry (DPV). This work introduced a first-time combination of graphene oxide (GO) with silicon dioxide (SiO$_2$) and the conducting polymer polyaniline (PANI) to improve dopamine detection. The composite material was synthesized using an *in situ* polymerization process, ensuring uniform integration of GO/SiO$_2$ with PANI. The GO/SiO$_2$@PANI-modified glassy carbon electrode (GCE) demonstrated a notable electrocatalytic activity for dopamine detection using DPV and CV. The performance of the sensor was evaluated across a range of dopamine concentrations, showing a linear detection range between 2 and 12 μM with a detection limit of 1.7 μM and relative standard deviation of 2.5%. The material's performance was attributed to the combined effects of graphene's surface area, PANI's conducting properties, and the structural integrity provided by SiO$_2$ nanoparticles (NPs). Additionally, the sensor's robustness and high selectivity were confirmed through tests with synthetic urine samples, where dopamine concentrations were detected with high accuracy. This work provides a promising avenue for the development of low-cost and efficient dopamine sensors for clinical applications.

Introduction

Dopamine is a nitrogen-containing organic compound with a catechol nucleus (a benzene ring with two hydroxyl groups) and an ethylamine side chain. It functions as a crucial neurotransmitter produced by neurons in the central nervous system, facilitating communication between neurons by relaying signals across synapses.[1] The imbalance of dopamine in the body can significantly impact mental, emotional, and physical health, leading to disorders like Parkinson's disease, schizophrenia, restless leg syndrome (RLS), and attention deficit hyperactivity disorder (ADHD).[2–4] Dopamine is commonly found in biological fluids such as urine and serum, making these fluids valuable for assessing its concentration.[5] Early measurement of dopamine in clinical samples can provide key insights into various neurological disorders, aiding in the timely diagnosis and treatment of the diseases.

Numerous methods have been established for the detection of dopamine like chemiluminescence,[6] high performance liquid chromatography-mass spectrometry (HPLC-MS),[7] spectrophotometry,[8] fluorometry,[9] capillary electrophoresis (CE),[10] electrochemical methods,[11] *etc.* The above-mentioned methods have practical drawbacks. HPLC is expensive, requiring large amounts of pure organic solvents, a proper power source, and regular maintenance.[12] Spectrophotometry and fluorometry methods are limited by the need for chromophores and fluorophores, requiring complex formation between the analyte and a reagent to produce colour, which adds complexity and may limit their applicability to certain analytes.[13] CE has sensitivity and control challenges, while electrochemical methods are cost-effective, simple, rapid, highly sensitive, and enable real-time monitoring. Electrochemical methods surpass HPLC, spectrophotometry, and CE in cost-effectiveness, simplicity, and speed. They require minimal reagents, offer high sensitivity, and enable real-time monitoring of analytes in complex samples directly at the source.

Electrochemical methods, such as cyclic voltammetry (CV), linear sweep voltammetry (LSV), differential pulse voltammetry (DPV) commonly use modified glassy carbon electrode (GCE) as a sensing probe for measurement of chemical substances in variety of samples.[14–16] In addition, electrochemical methods also employed for advanced technological applications such as wearable sensors and point of care diagnosis.[17] The bare GCE

School of Studies in Chemistry, Pt. Ravishankar Shukla University, Raipur, CG, 492010, India. E-mail: kshrivas@gmail.com

† Electronic supplementary information (ESI) available. See DOI: https://doi.org/10.1039/d5ra00714c

was unable to detect the dopamine and therefore modification of the electrode surface is needed. Thus, graphene oxide (GO) nanomaterials (NMs) on GCE were modified to enhance the larger surface area and exploited for determination of dopamine. Gao & research group employed a GO-modified GCE for dopamine detection, using a covalent functionalization process to modify the electrode. Other limitations include potential stability issues, less electron transfer (due to presence of sp^3 C), less uniformity and the complexity of synthesis and functionalization processes. Thangamuthu et al. explored the potential of graphene and graphene oxide (GO) in electrochemical sensing applications for biomolecule detection.[18,19] Further, GO–metal oxide (MO) nanoparticles (NPs) were used for detection of dopamine. The use of GO–MO NPs offers several advantages over graphene oxide alone, including enhanced electrochemical activity, improved stability, and increased surface area for binding target molecules.[20,21] Cai et al. developed Fe_2O_3/GO nanohybrids for dopamine detection, where α-Fe_2O_3 NPs were synthesized using a metal-ion mediated hydrothermal method, followed by the formation of an α-Fe_2O_3/GO composite through ultrasonication. They attributed the enhanced electrocatalytic oxidation of dopamine to the increased surface defects. In another study, Anbumannan et al. utilized a GO/WO_3-modified GCE for dopamine analysis, synthesizing the GO/WO_3 nanocomposite via a co-precipitation method. The incorporation of WO_3 NPs into the GO structure improved charge transfer and introduced surface defects, resulting in enhanced dopamine sensing.[22,23] GO–MO NMs face limitations in electrochemical detection due to potential agglomeration, reduced conductivity from metal oxide interactions, and sensitivity to environmental factors affecting stability and performance.

Recently, GO with MO NMs and conducting polymers significantly enhance electrochemical dopamine detection. Conducting polymers facilitate electron transfer, while MO NPs provide abundant active sites, improving sensitivity and selectivity by catalysing dopamine amidst interferents. These nanocomposites offer high electrocatalytic activity, stability, and reproducibility. Their ease of synthesis, modification, and scalability makes them cost-effective for practical applications in dopamine sensing.[24,25] Additionally, conductive Ni based metal–organic framework (MOFs) can be used in electrochemical sensing of glucose. MOFs are a combination of metal centre and organic linkers. MOFs based composite materials are widely used for electrochemical sensing of glucose because of its customizable chemical properties. Regulators are used for control synthesis of Ni-MOFs which further affects the size and shape of MOFs.[26–28]

Herein, cost-effective and selective electrochemical sensor using a GO, silicon dioxide (SiO_2), and polyaniline (PANI) composite for dopamine detection in clinical applications. This study investigated the detection sensitivity and selectivity of dopamine by combining GO's surface area, SiO_2's structural stability, and PANI's conductive properties. The GO/SiO_2@PANI composite aims to detect low concentrations of dopamine reliably, addressing current limitations in existing methods, such as high costs and complex fabrication processes.

Additionally, this study intends to validate the sensor's performance in synthetic urine to demonstrate its applicability for real-world clinical settings, enabling reliable monitoring of dopamine levels for neurological diagnostics.

Experimental section

Materials and solution preparations

Tetraethylorthosillicate (TEOS), ethanol (C_2H_5OH, $\geq$99%), ammonium hydroxide (NH_4OH), graphite flakes, sulphuric acid (H_2SO_4, $\geq$98%), sodium nitrate ($NaNO_3$) and sodium dodecyl sulphate (SDS), potassium permanganate ($KMnO_4$), hydrogen peroxide (H_2O_2), sodium sulphide (Na_2S), aniline ($C_6H_5NH_2$ $\geq$99.5%), hydrochloric acid (HCl), ammonium persulphate (($NH_4)_2S_2O_8$) and dopamine hydrochloride ($C_8H_{11}NO_2HCl$, 98%) and synthetic urine were purchased from Sigma-Aldrich (USA). All of the chemicals were of the highest quality for analytical grade. A 1 mM stock standard solution of dopamine was initially prepared in 50 mL double distilled water (DW) and working standard solutions were prepared by the appropriate dilution of standard solution and maintained the pH to 7.4 with 0.1 M phosphate buffer saline (PBS).

Instrumentation

All the electrochemical analysis were performed in electrochemical workstation, Solo (Admiral Squidstat, USA). Electrochemical cell included the three-electrode system where GCE was working electrode, platinum electrode was counter electrode, and Ag/AgCl was reference electrode. Fourier transform infrared (FTIR) spectroscopy (Nicolet-10, Thermo Scientific, USA) was employed to determine the surface modification of SiO_2 with GO/PANI to know the functional groups present on the surface of NMs. The synthesis of SiO_2 with GO/PANI was also confirmed using UV-visible spectrophotometer, Evolution-300 (Thermo Scientific, USA). X-ray photo electron spectroscopy (XPS) from NEXA G2, Thermo Scientific (USA) was exploited for determination of chemical composition and oxidation states. The Brunauer–Emmett–Teller (BET) method, using the BELSORP-maxII instrument was employed to evaluate the surface area and pore size distribution. Field emission-scanning electron microscope (FE-SEM) from Gemini SEM 500 KMAT (Carl Zeiss, Germany) was used for recording the morphological images of NMs.

Synthesis of GO/SiO_2@PANI

SiO_2 NPs were prepared using a hydrothermal method, with slight modifications to a previously reported procedure.[29] First, a 50 mL solution of ethanol and water, in equal volumes (25 mL each), was prepared and stirred continuously. Subsequently, 3.9 mL of TEOS was added to the solution, which already contained 1.5 g of SDS. The mixture was stirred for 30 min, followed by the gradual addition of 10 mL of NH_4OH while stirring until a white precipitate formed. This solid product was transferred into a hydrothermal reactor and heated at 140 °C for 24 h. After cooling, the solid was thoroughly washed with deionized water

to remove residual SDS. The final product was then rinsed with 30 mL of both ethanol and acetone and dried at 105 °C for 24 h.

GO was synthesized following a modified Hummers' method.[30] Briefly, 2 g of graphite flakes and 1.5 g of sodium nitrite were mixed with 69 mL of H_2SO_4 in a round-bottom flask, which was kept in an ice bath to maintain the temperature below 10 °C. The oxidation was initiated by slowly adding 9 g of $KMnO_4$ to the mixture. After 1 h, the reaction vessel was transferred to a silicone oil bath, and an additional 9 g of $KMnO_4$ was carefully added over the course of 7 h, while maintaining a temperature of approximately 35 °C. After 24 h, 3 mL of H_2O_2 was introduced to ensure complete oxidation. The mixture was then diluted by adding 400 mL of ice-cold water with constant stirring. The solution was centrifuged and washed multiple times with ultrapure water until a neutral pH was obtained. Finally, the suspension was rinsed with ethanol and dried in a Petri dish to yield GO sheets.

The *in situ* polymerization of aniline in the presence of SiO_2 NPs and GO was carried out using a chemical oxidative polymerization method. First, appropriate amounts of GO and SiO_2 NPs were dispersed in 50 mL of a 0.1 M HCl solution, and the mixture was stirred for 30 min using a magnetic stirrer. After 30 min, 0.9 mL of aniline was added to the solution, and stirring was continued for 15 min to ensure uniform distribution of the aniline. To initiate the polymerization, a 0.125 M solution of $(NH_4)_2S_2O_8$ was added dropwise to the mixture until an emerald green color appeared. To ensure complete polymerization of the PANI granules, the mixture was kept at 10 °C for 24 h. Afterward, the product was washed with 0.1 M HCl and acetone to remove any unpolymerized aniline.[29] Fig. 1(a) illustrate the synthesized

GO/SiO_2@PANI composite material for electrochemical sensing application.

Electrode modification

To develop the GO/SiO_2@PANI electrochemical biosensor, the GCE was first polished with 10 μm alumina powder. Next, the electrode was cleaned using ultrasonic waves in ethanol and deionized water for 2 min to achieve a highly reflective surface. *N*-methyl pyrrolidone was employed as a dispersing agent to produce a 250 μL suspension of GO/SiO_2@PANI, which was treated with ultrasonication for 30 min. Subsequently, a 5 μL drop of the GO/SiO_2@PANI suspension was placed on to the clean GCE, and left to dry for 4 h under an infrared lamp, resulting the formation of the GO/SiO_2@PANI/GCE biosensor, shown in Fig. 1(b).

Procedure for analysis of dopamine using the GO/SiO_2@PANI as an electrochemical sensor in DPV and CV

The electrocatalytic oxidation behaviour of dopamine was examined using DPV. The dopamine detection was carried out in a three-electrode electrochemical cell across a concentration range of 0.5 μM to 12 μM in a phosphate-buffered saline (PBS) solution at pH 7.4. An adsorptive DPV measurements were recorded by applying a potential from −0.5 V to 0.5 V, with an incremental potential step of 5 mV. The pulse parameters were set as follows: pulse amplitude of 0.05 V, pulse interval of 0.25 s, and pulse width of 0.50 s and scan rate was set as 100 mV s^{-1}. A single anodic peak corresponding to dopamine oxidation was
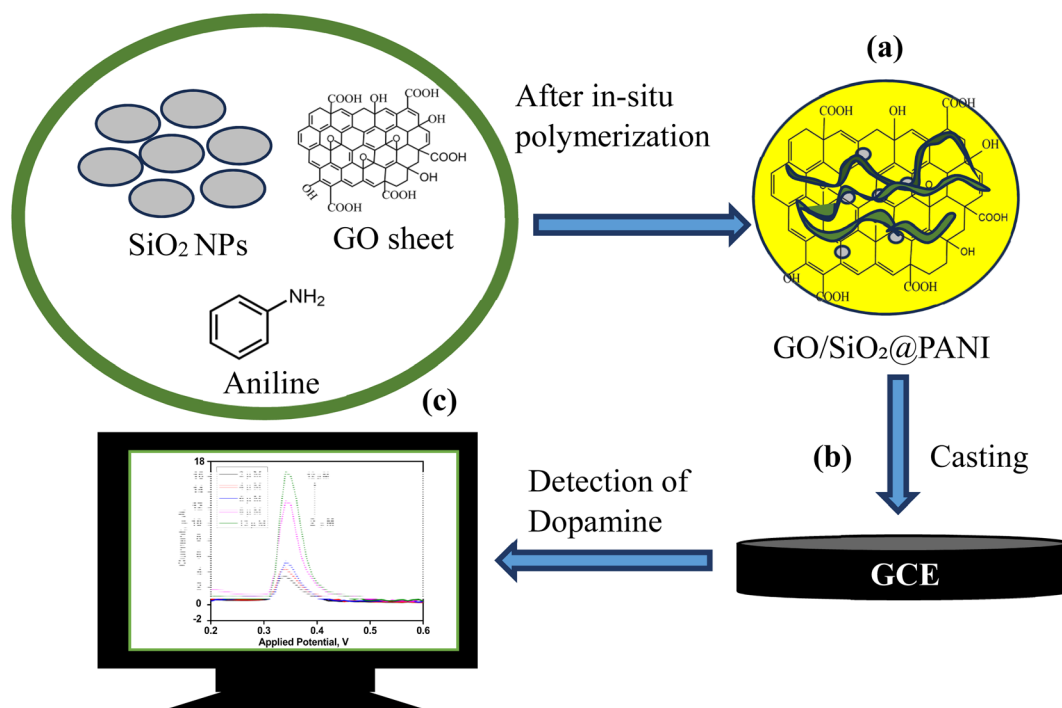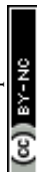

Fig. 1 (a) Synthesis of GO/SiO_2@PANI, (b) fabrication of GO/SiO_2@PANI on GCE electrode surface, and (c) detection of dopamine using GO/SiO_2@PANI as an electrochemical sensor.

observed at 0.34 V. The measurement of dopamine in electrochemical workstation is demonstrated in Fig. 1(c).

Results and discussion

Characterization of GO/SiO$_2$@PANI nanocomposite

UV-vis spectroscopy was employed for the initial confirmation of the material synthesis. Fig. 2(a) shows the UV-vis spectrum of GO–SiO$_2$ nanocomposite successfully integrated with PANI. The composite exhibited two absorption peaks, one between 230 and 350 nm and another from 450 to 750 nm. In contrast, SiO$_2$ alone displayed a single peak at 250 nm, confirming the formation of SiO$_2$ NPs.[31] The broad peak observed between 450 and 750 nm was attributed to the quinoid rings of PANI, indicating successful interaction between GO and PANI.[32] Fig. 2(b) represents the IR spectrum of GO, SiO$_2$ & GO/SiO$_2$@PANI where broad absorption band in the range of 3200–2000 cm^{-1}, corresponds to alcohol groups on the surface, along with two peaks between 1750 and 1650 cm^{-1} which are associated with ketone and carboxyl groups of the GO.[33] The IR spectrum of SiO$_2$ exhibited characteristic peaks at 1230 cm^{-1} and 800–900 cm^{-1} representing stretching and bending vibration of Si–O–Si group.[34] Further, the IR spectrum of the GO/SiO$_2$@PANI composite reveals that a broad peak in the 3200–2000 cm^{-1} range was still present, but with lower intensity, suggesting interaction between PANI and the surface functional groups (acid, ketone, alcohol) during *in situ* polymerization. FE-SEM was used to examine the surface morphology, distribution, and interaction of the components in the synthesized material, Fig. 2(c) and (d). The SEM image of SiO$_2$ NPs demonstrated their spherical shape, uniformity, and porous structure, Fig. 2(e). The TEM image of GO/SiO$_2$@PANI shown in Fig. 2(f) revealed a nanostructure with a large surface area. Thus,
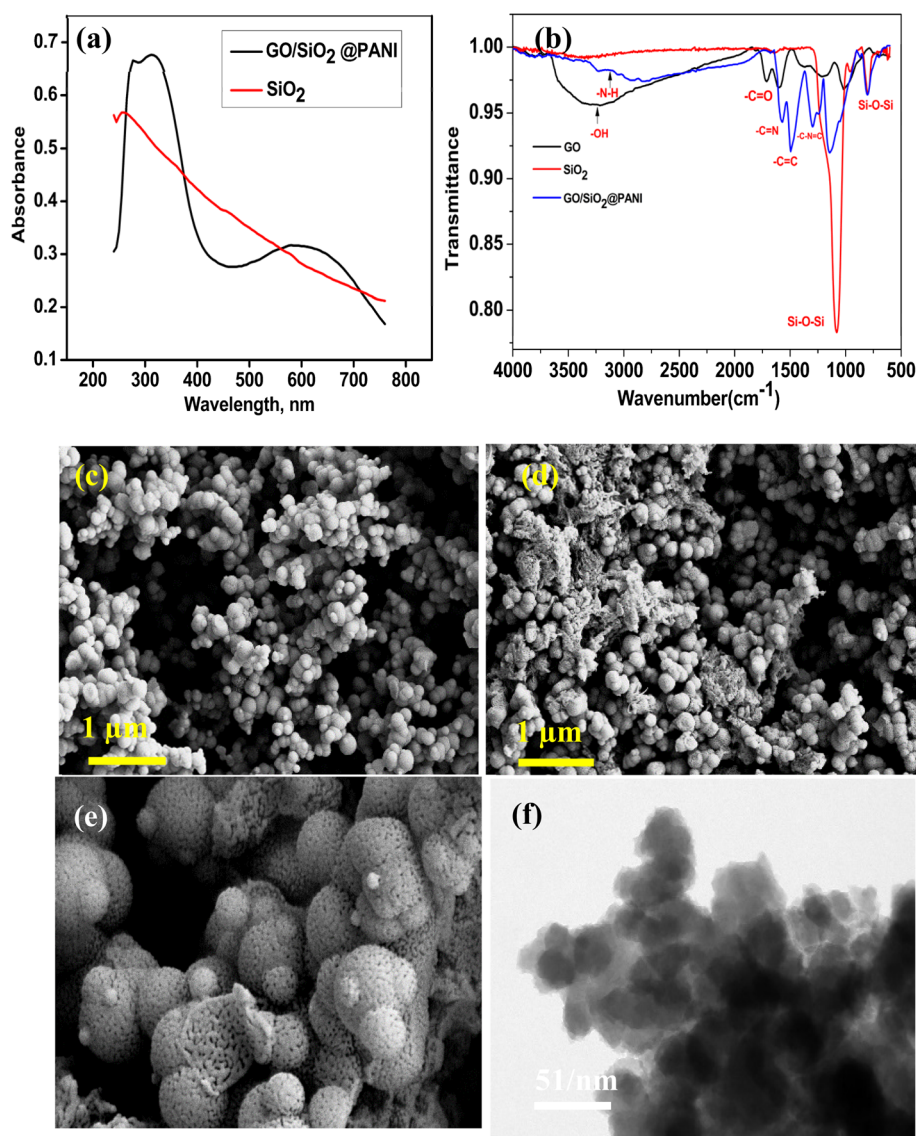

Fig. 2   (a) Shows the UV-vis spectra for GO/SiO$_2$@PANI and SiO$_2$ NPs, (b) shows the FTIR spectra of GO, SiO$_2$ NPs and GO/SiO$_2$@PANI, (c) showing the SEM image of SiO$_2$ NPs, (d) showing the FE-SEM image of GO/SiO$_2$@PANI, (e) enlarge view of SiO$_2$ NPs, (f) HR-TEM of GO/SiO$_2$@PANI.

SEM and TEM images of the composite indicated successful embedding of PANI and GO layers onto the surface of SiO₂ for electrochemical applications.[29]

Further, the full wide scan of XPS analysis of GO/SiO₂@PANI composite is shown in Fig. S1(a).† Additionally, the XPS spectra of C 1s, O 1s, N 1s, and Si 2p are given in Fig. S1(b)–(e).† The deconvoluted Si 2p spectrum displayed two peaks, one at 103.78 eV, corresponding to a small Si–O group, and another stronger peak at 102.38 eV, indicating C–Si interaction in the composite. The peaks (Fig. S1(e)†) at 103.78 eV and 102.38 eV indicated the oxidation states of silicon as Si(IV) and Si(II), respectively.[29] The C 1s deconvoluted peak showed the presence of various carbon functional groups, including C=C (284.48 eV) for sp^2 carbon, C–C/C–H (285.48 eV) for sp^3 carbon, C=O (287.78 eV) for sp^2 carbon bonded to oxygen, and O–C=O (291.18 eV) for carboxylic C–O.[35] XPS peak at 287.78 eV strongly suggesting the electrostatic interaction between the COOH group of GO with PANI. The N 1s spectrum revealed three peaks, one at 401.18 eV for pyridinic nitrogen, another at 400.48 eV for the imine (C=N) group, and a third at 399.58 eV for the amine (C–N) group.[36] The O 1s spectrum displayed peaks at 533.18 eV, 532.58 eV, and 531.38 eV, corresponding to C–O–H, C–O, and C=O, respectively.[37] These results confirmed that the successful incorporation of PANI onto the GO/SiO₂ composite.

BET analysis was conducted to determine the surface area and pore size of the GO/SiO₂@PANI. The results revealed a specific surface area of 56.88 m² g⁻¹ and a pore size of 11.22 nm. The adsorption–desorption isotherm, pore size distribution plot, and corresponding data are presented in Fig. S2 and Table S1.† These findings suggest that the GO/SiO₂@PANI composite possesses an adequate surface area to facilitate effective dopamine adsorption at the electrode surface.

Electrochemical performance of GO/SiO₂@PANI for detection of dopamine

To investigate the performance of different electrode materials, DPV was carried out using the modified electrode. The electrochemical performance of NMs, including SiO₂, SiO₂/GO, SiO₂/PANI, GO/PANI, and GO/SiO₂@PANI, modified on a GCE for dopamine detection, is illustrated in Fig. 3(a). The SiO₂-modified electrode exhibited some sensitivity toward dopamine detection. Its surface area and free energy facilitated dopamine immobilization, enhancing its interaction with the electrode. Incorporating GO into the electrode along with PANI led to a significant increase in the peak current. The oxygenated functional groups in GO interacted with dopamine, improving its adsorption on the surface. Furthermore, PANI, being a conductive polymer, facilitated efficient electron transfer between the electrode and the analyte. The π–π interactions between dopamine's phenyl ring and the PANI–GO composite further enhanced the electron transfer efficiency, resulting in higher peak currents. Among the modified electrodes, GO/SiO₂@PANI exhibited the highest peak current, indicating superior electrochemical performance for dopamine detection. The synergistic effect of GO, SiO₂, and PANI contributed to enhanced surface area, improved conductivity, and efficient dopamine adsorption, making it an ideal electrode material for sensitive electrochemical sensing.[38–40]

In addition, the electrochemical impedance spectroscopy (EIS) was conducted to evaluate and compare the electron transfer kinetics at the electrode–electrolyte interface for SiO₂, GO/PANI, and GO/SiO₂@PANI-modified electrodes. The EIS analysis for dopamine detection using these modified GCEs is presented in Fig. 3(b). EIS measurements were performed in a 5 mM potassium ferrocyanide solution prepared in 0.1 M KCl. The results revealed that the GO/SiO₂@PANI-modified electrode exhibited better conductivity. This enhanced conductivity can be attributed to the synergistic effect of GO, SiO₂, and PANI, which facilitated efficient charge transfer and improved electron mobility at the electrode surface.[41]

Thus, the GO/SiO₂@PANI composite electrode demonstrated the highest peak current, outperforming the other two. The combination of GO, PANI, and SiO₂ created a synergistic effect. GO increased the surface area and adsorption capacity, while PANI facilitated electron transfer, and SiO₂ contributed to dopamine immobilization. This composite material leveraged the advantages of each component, yielding the most effective performance for dopamine detection in terms of both sensitivity and peak current. Thus, the GO/SiO₂@PANI modified GCE provided superior electrochemical performance, making it the best candidate for dopamine sensing.
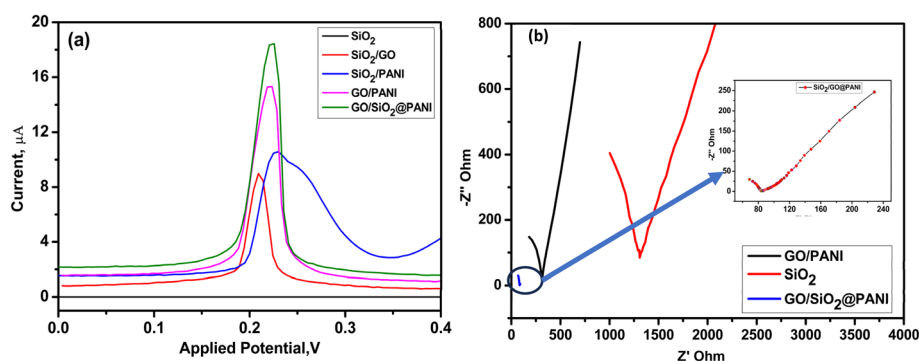

Fig. 3 (a) Shows the differential pulse voltametric sensing of dopamine of 12 μM concentration using SiO₂, SiO₂/GO, SiO₂/PANI, GO/PANI and GO/SiO₂@PANI modified GCE (PBS buffer) (b) EIS analysis of 5 mM of K₄[Fe (CN)₆] with 0.1 M KCl using GO/PANI, SiO₂ and GO/SiO₂@PANI to determine the charge transfer resistance.

Optimization of electrochemical detection of dopamine

The optimization of the pH of the solution is a crucial factor for better electrochemical response of dopamine using GO/SiO$_2$@PANI modified GCE as an electrochemical sensor. The influence of pH on the dopamine oxidation peak was evaluated using DPV, with pH values ranging from 3.0 to 9.0. The results are shown in Fig. S3(a).† The optimum detection was observed at pH 7.0 and further increase in the pH of solution caused the decrease in the signal response. Thus, pH 7.0 was utilized for performing all the experiments. At pH (7.0), dopamine exists in a protonated form, leading to strong electrostatic attraction and oxidation *via* oxygenated functional groups at this pH. Huang *et al.* confirmed that near-neutral pH facilitates interaction between negatively charged GO and positively charged dopamine, significantly enhancing the interaction between GO and dopamine.[42] The deposition time is also essential to ensure complete deposition on the electrode surface for effective detection of target analyte. This was done by immersing the electrode in a 12 μM dopamine solution from 1 to 8 min, illustrated in Fig. S3(b).† The deposition time of 6 min was sufficient to deposited on the electrode surface for better detection of dopamine.[40]

Mechanism for electrochemical detection of dopamine using GO/SiO$_2$@PANI/GCE as an electrochemical sensor

The detection mechanism of dopamine using a SiO$_2$/GO@PANI-modified electrode involved the several key processes, demonstrated in Fig. 4(a). When the electrode was immersed in a dopamine solution, dopamine molecules adsorbed onto the electrode surface, increasing the local concentration of dopamine at the interface. As the electrode became fully saturated with dopamine, all active sites were occupied, which contributed to a stable and distinct oxidation peak in DPV. GO played a crucial role due to its oxygen-containing functional groups, such as carboxyl (–COOH), epoxy, and hydroxyl (–OH). These groups facilitated the electrostatic interactions with the protonated amine group (–NH$_3^+$) of dopamine. This interaction enhanced the adsorption of dopamine onto the electrode surface, further increasing the local concentration of dopamine. Moreover, the oxygen-containing groups in GO can lower the electron density within the graphene structure, improving the electrode's oxidizing capabilities. This allowed for more efficient electron transfer from dopamine to the electrode during the oxidation process, resulting in a well-defined and pronounced oxidation peak in the DPV signal.[43,44] This enhanced electron transfer is a key factor in the sensitive detection of dopamine using the SiO$_2$/GO@PANI electrode.

Further, CV study was also performed at different scan rates (10–100 mV s^{-1}) for electrochemical detection using GO/SiO$_2$@-PANI-modified electrode. As shown in Fig. 4(b), both anodic and cathodic peak currents increased proportionally with scan rate, indicating a typical redox behaviour. The well-defined and symmetric peaks suggest a reversible or quasi-reversible process with efficient electron transfer kinetics at the electrode surface. Notably, a linear relationship was observed between the logarithm of anodic peak current and the logarithm of scan rate (Fig. 4(c)), with a slope of 0.8175 and a high correlation coefficient
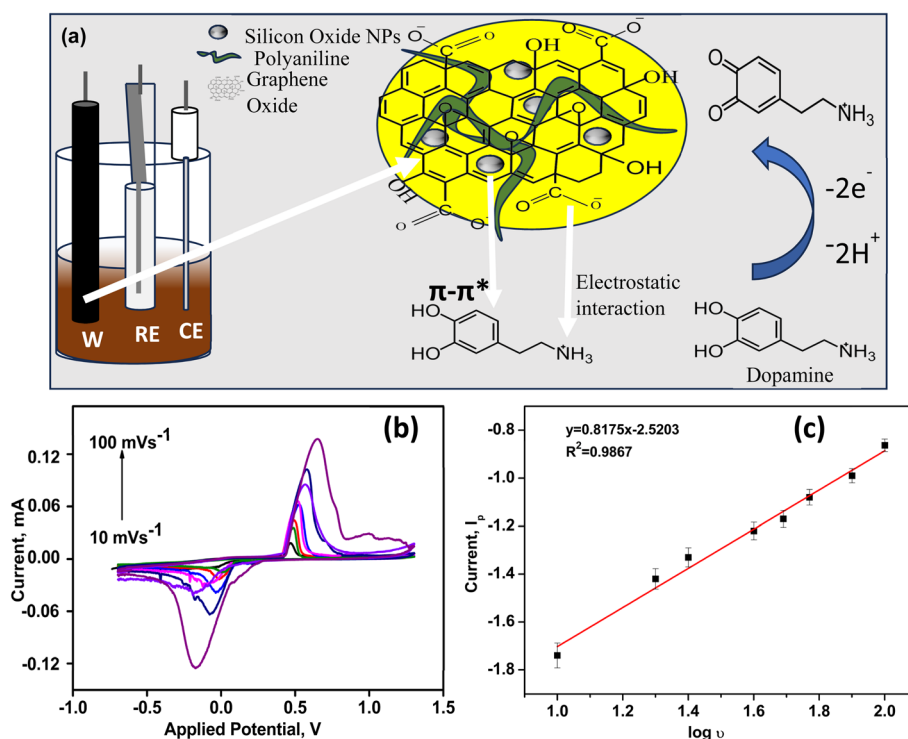

Fig. 4 (a) Scheme demonstrate the mechanism for detection of dopamine using GO/SiO$_2$@PANI as an electrochemical sensing probe that were fabricated on the GCE; (b) CVs of 12 μM/0.1 M PBS buffer (pH = 7.4) at GO/SiO$_2$@PANI at different scan rate from 10–100 mV s^{-1} (c) showing the result of variation of log of oxidation peak current for 12 μM concentration of dopamine *versus* log of scan rate.

($R^2 = 0.9867$), confirming that the redox process is primarily adsorption-controlled. Additionally, with increasing scan rate, the anodic peak potential gradually shifts toward more positive values, further supporting that the electrochemical process at the electrode surface is adsorption-controlled.[45,46]

Analytical evaluation for determination of dopamine using GO/SiO₂@PANI as electrode

The analytical evaluation of dopamine determination using the GO/SiO₂@PANI-modified GCE using DPV demonstrated a reliable and precise method for dopamine detection. The linear range for dopamine was established between 2 and 12 μM, with the analysis performed by spiking dopamine into a pH 7.4 buffer and recording the voltammograms, illustrated in Fig. 5(a). The potential was swept from −0.5 V to +0.5 V, and a clear linear relationship was observed between the anodic oxidation peak current and the increasing dopamine concentration. This is further supported by the calibration curve Fig. 5(b), which yielded a correlation coefficient (R^2) of 0.995, indicating excellent linearity within the tested concentration range.[47]

The method's sensitivity is reflected in the limit of detection (LOD) and LOQ, which was found to be 1.7 μM and 5.5 μM, respectively, demonstrating the electrode's capability to detect low concentrations of dopamine. Additionally, the inter-day and intra-day precision of the method was evaluated through the relative standard deviation (RSD%) of the oxidation peak current, which was found to be 3.4 and 2.5% respectively, showing good reproducibility for dopamine detection. Furthermore, the same concentration of dopamine was analysed on the 1st, 10th, 20th, and 30th days using GO/SiO₂@PANI electrode. No significant change in the DPV peak currents was observed over this period, indicating long-term stability of the electrode Fig. S4.† These findings demonstrate that the oxidation peak remains consistent and can be reliably used for the determination of dopamine in unknown clinical samples.

Furthermore, several biomolecules such as glucose, uric acid, and ascorbic acid may present in clinical samples cause the interference in analysis of dopamine. Thus, 1.0 mM of these substances were individually spiked and in the presence of these substances, dopamine was determined using DPV. The results are shown in Fig. S5.† No DPV peaks associated with these matrix substances were observed within the given potential range of target analyte, indicating that dopamine can be selectively detected even in the presence of these complex matrix components.

Application of the GO/SiO₂@PANI as an electrochemical sensor for determination of dopamine in synthetic urine sample

SiO₂/GO@PANI modified electrode was exploited for electrochemical measurement of dopamine in clinical samples to investigate the reliability of the method. For this, synthetic urine was analysed in DPV under the optimized conditions with 0.1 M (7.4 pH). The oxidation peak was considered for measurement of dopamine present in unknown urine samples using the standard calibration curve. The dopamine concentration in urine sample was 3.5 μM using GO/SiO₂@PANI as an electrochemical sensor. In addition, the accuracy of dopamine determination in urine samples can be assessed by calculating the relative recovery percentage. This involves spiking known concentrations of dopamine (2 μM and 5 μM) into the urine sample, followed by measuring the dopamine concentration using an analytical method, such as electrochemical detection. The relative recovery (%) is calculated by comparing the measured concentration of dopamine in the spiked sample to the concentration (spiked amount + endogenous amount). A recovery percentage close to 100% indicates high accuracy, ensuring that the method reliably quantifies dopamine in urine without significant matrix interference.

Comparison of the SiO₂/GO@PANI for determination of dopamine with other reported methods

Table 1 represents the comparison of present method with previously reported work on the dopamine detection using various electrochemical techniques. The applicability of the prepared electrode material for detection of dopamine using adsorptive DPV was compared with the other method such as MCPE-GO/DPV,[48] CNT-N/DPV,[49] GR-SnO₂/DPV,[50] RGO/AuNPs/DPV,[51] AuNPs@PANI/DPV,[52] GO/TiO₂/DPV[53] in terms of the functional electrode material, electrochemical methods, linearity range, LOD. However, variations in the composition during the preparation of the modified carbon paste electrode (M-CPE) led to fluctuations in current values during the experiment.[58] The carbon ionic liquid electrode (CILE), previously reported, offered
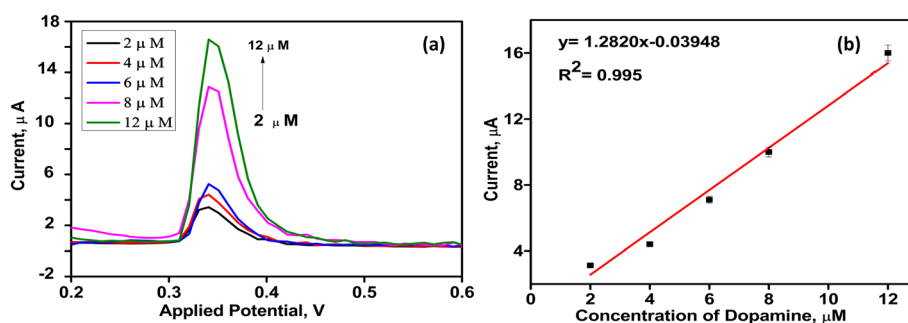

Fig. 5 (a) DPV peaks for different concentrations of dopamine from 2 to 12 μM with PBS buffer (pH 7.4) and (b) standard calibration curve for respective dopamine concentrations.

Table 1 Comparison for determination of dopamine using GO/SiO₂@PANI electrochemical sensor with other reported methods

Functional materials	Methods	Range of linearity, μM	LOD, μM	Samples	Ref.
MCPE-GO	DPV	0.7–70	0.15	Blood serum	48
CNT-N	DPV	1–20	—	—	49
CILE-GR-SnO₂	DPV	0.5–500	0.13	Injection sample	50
RGO/AuNPs	DPV	0.14–700	0.14	—	51
AuNPs@PANI	DPV	10–1700	5	Human serum	52
GO/TiO₂	CV	0.2–10	0.03	Human urine	53
GO/PANI	CV	2–18	0.5	Aqueous solution	54
	DPV				
Ferrocene-Pd-ormosil	Amperometry	—	50	Aqueous solution	55
PNT-[Cu₄(apyhist)₄]⁴⁺/Nafion	SWV	5–40	2.80	Aqueous solution	56
PNCPy & PNMPy	CV	1000–10000	300	Aqueous solution	57
GO/SiO₂@PANI	DPV	2–12	1.7	Synthetic urine	Present work

high conductivity, making it suitable for analyte sensing in electrochemical analysis. However, it had several drawbacks, including high cost, high viscosity, and a tendency to absorb moisture.[59] Another material, GO/TiO₂, exhibited decent electrical conductivity, but its surface functionalization properties were poor due to inadequate binding interactions with the analyte, likely caused by its photocorrosive nature.[60] Subsequently, the electrode modified with AuNPs also has limitations like high cost, lower stability under certain conditions.[61] Key material GO/PANI, showed good response for electrochemical detection of dopamine but the composite stability will be less without the MO NPs because of the chances of agglomeration. The incorporation of MO NPs into the composite of GO/PANI enhances the stability of the composite.[54] The present method was found better than the NMs such as AuNPs@PANI,[52] Ferrocene-Pd-ormosil,[55] and PNT-[Cu₄(apyhist)₄]⁴⁺/Nafion,[56] PNCPy & PNMPy,[57] used for electrochemical detection of dopamine in different clinical samples.

Conclusions

Herein, GO/SiO₂@PANI nanocomposite-based sensor was developed for the electrochemical detection of dopamine in synthetic urine. The combination of GO, SiO₂, PANI leveraged each component's properties—GO's surface area, SiO₂'s structural stability, and PANI's conductivity—to achieve high sensitivity and selectivity in dopamine detection. The sensor demonstrated a reliable linear detection range with a low limit of detection, making it effective for clinical applications. The application in synthetic urine confirmed its robustness and accuracy, even in complex sample matrices. Compared to existing methods, the GO/SiO₂@PANI sensor offers a more cost-effective, stable, and efficient approach. This composite-based sensor presents a promising alternative for practical, low-cost dopamine monitoring, supporting early diagnosis and management of neurological disorders. The method's simplicity, selectivity, and reproducibility make it a valuable tool in clinical diagnostics.

Data availability

Data is provided as ESI.†

Conflicts of interest

There are no conflicts to declare.

Acknowledgements

References

1 A. E. Pereda, *Nat. Rev. Neurosci.*, 2014, **15**, 250–263.
2 M. O. Klein, D. S. Battagello, A. R. Cardoso, D. N. Hauser, J. C. Bittencourt and R. G. Correa, *Cell. Mol. Neurobiol.*, 2019, **39**, 31–59.
3 X. Liu and J. Liu, *View*, 2021, **2**, 20200102.
4 H. Kaur, S. S. Siwal, R. V. Saini, N. Singh and V. K. Thakur, *ACS Nanosci. Au*, 2023, **3**, 1–27.
5 E. Grouzmann and F. Lamine, *Best Pract. Res. Clin. Endocrinol. Metabol.*, 2013, **27**, 713–723.
6 Y. Lan, F. Yuan, T. H. Fereja, C. Wang, B. Lou, J. Li and G. Xu, *Anal. Chem.*, 2019, **91**, 2135–2139.
7 V. Carrera, E. Sabater, E. Vilanova and M. A. Sogorb, *J. Chromatogr. B*, 2007, **847**, 88–94.
8 N. O. A. Al-Salahi, E. Y. Hashem and D. A. Abdel-Kader, *Spectrochim. Acta, Part A*, 2022, **278**, 121278.
9 X. Liu, W. Zhang, L. Huang, N. Hu, W. Liu, Y. Liu, S. Li, C. Yang, Y. Suo and J. Wang, *Microchim. Acta*, 2018, **185**, 234.
10 K. Vuorensola, H. Sirén and U. Karjalainen, *J. Chromatogr. B*, 2003, **788**, 277–289.
11 D. Yu, Y. Zeng, Y. Qi, T. Zhou and G. Shi, *Biosens. Bioelectron.*, 2012, **38**, 270–277.
12 Z. Wang, H. Guo, R. Gui, H. Jin, J. Xia and F. Zhang, *Sens. Actuators, B*, 2018, **255**, 2069–2077.
13 N. Thakur, D. Gupta, D. Mandal and T. C. Nagaiah, *Chem. Commun.*, 2021, **57**, 13084–13113.

14 S. Cheemalapati, S. Palanisamy, V. Mani and S.-M. Chen, *Talanta*, 2013, **117**, 297–304.

15 P. Sengupta, K. Pramanik and P. Sarkar, *Sens. Actuators, B*, 2021, **329**, 129052.

16 S. Zhu, H. Li, W. Niu and G. Xu, *Biosens. Bioelectron.*, 2009, **25**, 940–943.

17 M. A. Fathy and P. Bühlmann, *Biosensors*, 2025, **15**, 51.

18 F. Gao, X. Cai, X. Wang, C. Gao, S. Liu, F. Gao and Q. Wang, *Sens. Actuators, B*, 2013, **186**, 380–387.

19 M. Thangamuthu, K. Y. Hsieh, P. V. Kumar and G.-Y. Chen, *Int. J. Mol. Sci.*, 2019, **20**, 2975.

20 S. Kumar, S. D. Bukkitgar, S. Singh, Pratibha, V. Singh, K. R. Reddy, N. P. Shetti, C. Venkata Reddy, V. Sadhu and S. Naveen, *ChemistrySelect*, 2019, **4**, 5322–5337.

21 F. Parnianchi, M. Nazari, J. Maleki and M. Mohebi, *Int. Nano Lett.*, 2018, **8**, 229–239.

22 V. Anbumannan, R. T. R. Kumar and K. Suresh, *Mater. Sci. Semicond. Process.*, 2021, **127**, 105696.

23 Z. Cai, Y. Ye, X. Wan, J. Liu, S. Yang, Y. Xia, G. Li and Q. He, *Nanomaterials*, 2019, **9**, 835.

24 B. S. Dakshayini, K. R. Reddy, A. Mishra, N. P. Shetti, S. J. Malode, S. Basu, S. Naveen and A. V. Raghu, *Microchem. J.*, 2019, **147**, 7–24.

25 G. Kaur, A. Kaur and H. Kaur, *Polym.-Plast. Technol. Mater.*, 2021, **60**, 504–521.

26 P. Li, Y. Bai, G. Zhang, X. Guo, X. Meng and H. Pang, *Inorg. Chem. Front.*, 2022, **9**, 5853–5861.

27 Q. Zhang, P. Li, J. Wu, Y. Peng and H. Pang, *Adv. Sci.*, 2023, **10**, 2304102.

28 R. Zhu, Y. Song, J. Hu, K. Zhu, L. Liu, Y. Jiang, L. Xie and H. Pang, *Chem.–Eur. J.*, 2024, **30**, e202400982.

29 R. Kumar, M. A. Barakat, M. A. Taleb and M. K. Seliem, *J. Cleaner Prod.*, 2020, **268**, 122290.

30 D. C. Marcano, D. V. Kosynkin, J. M. Berlin, A. Sinitskii, Z. Sun, A. Slesarev, L. B. Alemany, W. Lu and J. M. Tour, *ACS Nano*, 2010, **4**, 4806–4814.

31 N. Elizondo-Villarreal, E. Gandara-Martínez, M. García-Méndez, M. Gracia-Pinilla, A. M. Guzmán-Hernández, V. M. Castaño and C. Gómez-Rodríguez, *Coatings*, 2024, **14**, 919.

32 N. s. Ahmed, C.-Y. Hsu, Z. H. Mahmoud, H. Sayadi and E. kianfar, *RSC Adv.*, 2023, **13**, 36280–36292.

33 M. Bera, Chandravati, P. Gupta and P. K. Maji, *J. Nanosci. Nanotechnol.*, 2018, **18**, 902–912.

34 J. Tao, *J. Mater. Res.*, 2012, **27**, 2644–2649.

35 H. Wang, Q. Hao, X. Yang, L. Lu and X. Wang, *ACS Appl. Mater. Interfaces*, 2010, **2**, 821–828.

36 V. C. Valsalakumar, A. S. Joseph, J. Piyus and S. Vasudevan, *ACS Appl. Nano Mater.*, 2023, **6**, 8382–8395.

37 V. H. N. Martins, N. M. S. Siqueira, J. E. S. Fonsaca, S. H. Domingues and V. H. R. Souza, *ACS Appl. Nano Mater.*, 2021, **4**, 5553–5563.

38 D. Butler, D. Moore, N. R. Glavin, J. A. Robinson and A. Ebrahimi, *ACS Appl. Mater. Interfaces*, 2021, **13**, 11185–11194.

39 J. Tashkhourian and S. F. Nami-Ana, *Mater. Sci. Eng., C*, 2015, **52**, 103–110.

40 Y. Zeng, Y. Zhou, L. Kong, T. Zhou and G. Shi, *Biosens. Bioelectron.*, 2013, **45**, 25–33.

41 S. S. M. Hassan, M. A. Fathy, I. Moussa, M. Obaida and A. H. Kamel, *Sens. Actuators, B*, 2023, **380**, 133397.

42 S. Hu, Q. Huang, Y. Lin, C. Wei, H. Zhang, W. Zhang, Z. Guo, X. Bao, J. Shi and A. Hao, *Electrochim. Acta*, 2014, **130**, 805–809.

43 N. Roy, S. Yasmin and S. Jeon, *Microchem. J.*, 2020, **153**, 104501.

44 P. Wiench, Z. González, R. Menéndez, B. Grzyb and G. Gryglewicz, *Sens. Actuators, B*, 2018, **257**, 143–153.

45 M. Mahanthappa, V. Duraisamy, P. Arumugam and S. M. Senthil Kumar, *ACS Appl. Nano Mater.*, 2022, **5**, 18417–18426.

46 H. Filik, A. A. Avan, S. Aydar and R. B. Arpaci, *Int. J. Electrochem. Sci.*, 2014, **9**, 2775–2789.

47 N. F. Atta, A. Galal and D. M. El-Said, *ACS Omega*, 2019, **4**, 17947–17955.

48 T. Thomas, R. J. Mascarenhas, C. Nethravathi, M. Rajamathi and B. E. Kumara Swamy, *J. Electroanal. Chem.*, 2011, **659**, 113–119.

49 J. Zhao, W. Zhang, P. Sherrell, J. M. Razal, X.-F. Huang, A. I. Minett and J. Chen, *ACS Appl. Mater. Interfaces*, 2012, **4**, 44–48.

50 W. Sun, X. Wang, Y. Wang, X. Ju, L. Xu, G. Li and Z. Sun, *Electrochim. Acta*, 2013, **87**, 317–322.

51 C.-S. Lee, S. H. Yu and T. H. Kim, *Nanomaterials*, 2018, **8**, 17.

52 L. Yang, S. Liu, Q. Zhang and F. Li, *Talanta*, 2012, **89**, 136–141.

53 D. S. R. Josephine, K. J. Babu, G. p. Gnana kumar and K. Sethuraman, *Microchim. Acta*, 2017, **184**, 781–790.

54 P. Manivel, M. Dhakshnamoorthy, A. Balamurugan, N. Ponpandian, D. Mangalaraj and C. Viswanathan, *RSC Adv.*, 2013, **3**, 14428–14437.

55 P. C. Pandey, S. Upadhyay, I. Tiwari, G. Singh and V. S. Tripathi, *Sens. Actuators, B*, 2001, **75**, 48–55.

56 I. d. O. Matos and W. A. Alves, *ACS Appl. Mater. Interfaces*, 2011, **3**, 4437–4443.

57 G. Fabregat, E. Córdova-Mateo, E. Armelin, O. Bertran and C. Alemán, *J. Phys. Chem. C*, 2011, **115**, 14933–14941.

58 M. Forouzandeh, M. Heidariramsheh, H. R. Heydarnezhad, H. Nikbakht, M. Stefanelli, L. Vesce and N. Taghavinia, *Carbon*, 2024, **229**, 119450.

59 V. V. Singh, A. K. Nigam, A. Batra, M. Boopathi, B. Singh and R. Vijayaraghavan, *Int. J. Electrochem.*, 2012, **2012**, 165683.

60 J. Bogdan, A. Jackowska-Tracz, J. Zarzyńska and J. Pławińska-Czarnak, *Nanoscale Res. Lett.*, 2015, **10**, 57.

61 S. K. Balasubramanian, L. Yang, L.-Y. L. Yung, C.-N. Ong, W.-Y. Ong and L. E. Yu, *Biomaterials*, 2010, **31**, 9023–9030.